THE ASTROPHYSICAL JOURNAL, 384:423–432, 1992 January 10

ELLIPTICAL GALAXIES WITH DARK MATTER. I. SELF-CONSISTENT MODELS

G. BERTIN AND R. P. SAGLIA[1]
Scuola Normale Superiore, Piazza dei Cavalieri 7, 56126 Pisa, Italy
AND
M. STIAVELLI
European Southern Observatory, Karl-Schwarzschild-Strasse 2, D-8046 Garching bei München, Germany
Received 1991 January 29; accepted 1991 July 22

ABSTRACT

A large survey of two-component, spherically symmetric, collisionless, self-consistent models is carried out with the aim of studying elliptical galaxies embedded in massive dark halos. Although many factors and options are explored in quantitative detail, the main focus is on a family of models where the luminous component is mostly isotropic inside the half-light radius and the dark component is slightly warmer (and normally more diffuse) than the luminous component, consistent with the picture that ellipticals were generically formed as a result of collisionless collapse (or merging) in the presence of cold/warm dark matter. The constraints imposed by self-consistency are found to be quite complex, but a few important features (such as limits on the amount of dark matter inside the half-light radius in terms of observed quantities and a characterization of the physical parameter space) are clarified by a proper use of the Jeans equations and of the virial theorem. In spite of the variety of kinematical profiles realized in our self-consistent models, we note a natural "conspiracy" to support realistic photometries, that is, luminosity profiles consistent with the $R^{1/4}$ law. Within our main family of models, we develop the concept of "minimum-halo models" as a way to fit a given set of data by minimizing the request of dark matter. This paper, where many of the results are illustrated in terms of projected quantities for a direct application to observed objects, forms the theoretical basis for a systematic study of photometric and kinematical properties of elliptical galaxies that may give quantitative estimates on the amount of dark matter present in these systems.

Subject headings: dark matter — galaxies: elliptical and lenticular, cD — galaxies: fundamental parameters — galaxies: kinematics and dynamics

1. INTRODUCTION

Dynamical evidence for the presence of dark matter in galaxies is usually claimed when models with stellar components characterized by constant mass-to-light ratios prove inadequate when confronted with observations. The possibility of radial gradients in the M/L ratios for the stellar components is generally discarded especially because large color gradients are not observed (Peletier et al. 1990; Franx & Illingworth 1990). For spiral galaxies this point of view leads to the construction of "maximum-disk models" (see van Albada & Sancisi 1986); in general, significant amounts of dark matter are required only when the models are confronted with H I data well beyond the optical disk, as in the clear case of NGC 3198 (van Albada et al. 1985).

For elliptical galaxies the situation is less clear (see Sarazin 1987; Sancisi & van Albada 1987). Although one-component stellar dynamical models so far appear to provide a good zeroth-order description of current data (see, e.g., Bertin, Saglia, & Stiavelli 1988; van der Marel, Binney, & Davies 1990; Binney, Davies, & Illingworth 1990; Efstathiou, Ellis, & Carter 1982), the kinematical data considered for these galaxies are mostly restricted to the region inside the half-light radius. Indeed, nonstellar kinematic indicators that are sometimes available on a larger scale (such as X-rays or H I; see Forman et al. 1979; Fabricant, Lecar, & Gorenstein 1980; Canizares, Fabbiano, & Trinchieri 1987; Raimond et al. 1981; van Gorkom et al. 1986; Schweizer, van Gorkom, & Seitzer 1989; Lees, van Gorkom, & Knapp 1990) tend to favor the view that dark matter is present also in ellipticals. In particular, some cases of flat H I rotation curves have been found, raising the interesting possibility of a "kinematic conspiracy" similar to that found in spiral galaxies.

This brief discussion gives the primary motivation for this paper, that is, the construction of self-consistent two-component models of elliptical galaxies where one component is supposed to represent the stars and the other the dark matter. The theoretical issue addressed here in great detail is the role of self-consistency in constraining the properties of the models. Note that because of the Gauss theorem, we expect the distribution of dark matter, if diffuse, to suffer more from the influence of luminous matter than vice versa. On the other hand, if we are going to invoke the presence of dark matter based on some kinematical signatures on the stellar component, such as a relatively flat velocity dispersion profile (see Saglia, Bertin, & Stiavelli 1992, hereafter Paper II), we should consider the possibility that dark matter may be present in significant amounts inside the half-light radius and thus affect the distribution of the stellar component. Therefore, it is not clear *why* the luminosity profile should always conform to the universal $R^{1/4}$ law (de Vaucouleurs 1948, 1953) rather than being distorted depending on the amount of dark matter present; this seems to be a kind of "photometric conspiracy" operating if elliptical galaxies do indeed contain dark matter (Bertin, Saglia, & Stiavelli 1989). In fact, it is somewhat of a miracle that the realization and survival of the $R^{1/4}$ profile happen to occur for a large subset of the parameter space

[1] Postal address: Landessternwarte, D-6900 Heidelberg-Koenigstuhl, Germany.

defining our simple but fully self-consistent models (see especially following § 5).

There are two possibilities for distributing dark matter differently from the luminous component. One way is to consider dark halos with a *different shape* (see the extreme case of spiral galaxies where dark matter is thought to have a spheroidal distribution in contrast with the stellar disk); the other is to have a distribution with a *different radial scale length* (in particular a larger scale length). Although the first possibility raises many interesting questions, in this paper we shall address only the second aspect which can be tackled adequately already in the simplified context of spherical models.

The paper is organized in the following way. First we choose a form for the distribution function describing both components and justify the merits and limitations of our choice (§ 2). Then we discuss the properties of the large parameter space that characterizes the family of models of main interest (§ 3) and present our survey of models which leads to the construction of a "data base" of 2939 fully self-consistent models within the main family (§ 4); we illustrate the intrinsic and observable properties of the models found. In § 5, we develop the concept of *minimum-halo models*, derive a few simple expressions that relate the amount of dark matter inside the half-light radius to the observed stellar velocity dispersion profile, and discuss the properties of models with good luminosity profiles ("photometric conspiracy") in the physical parameter space. In Appendix A some of the adopted numerical techniques are briefly outlined with reference to the numerical accuracy that has been obtained, and to the completeness of the survey. Appendix B is devoted to an exploration of some issues that are beyond the main goal of this article, that is, rotation and properties of some models that are outside the main survey.

2. CHOICE OF THE DISTRIBUTION FUNCTION FOR THE TWO COMPONENTS

With the aim of studying the effects on the observable quantities of the introduction of a dark component in an equilibrium model of elliptical galaxy, we have constructed a family of fully self-consistent two-component models. In the physical picture where the two components are both collisionless and have undergone similar dynamical processes during galaxy formation starting from different initial conditions, we should consider two distribution functions (that may be taken to be of the same form, but to imply different scale lengths and masses for the dark and the luminous component), keeping in mind the empirical constraint that the luminous component should follow the $R^{1/4}$ law. In addition, given the little evidence available so far for the presence of dark matter inside elliptical galaxies, we would like to explore a range of models where the dark component is progressively "turned on" over a well-justified reference model with no dark matter. One such reference case is that of the f_∞-models (Bertin & Stiavelli 1984), which we have found to possess interesting properties in relation to the statistical mechanics of galaxy formation (Stiavelli & Bertin 1987) and to the detailed fit of observed galaxies (see Bertin et al. 1988). It should be noted that this approach is preferred over the simpler scheme of embedding a specified model for the luminous component in a "frozen" spherical halo since it enables one to investigate the problem of "photometric conspiracy" and to consider models where the two components have comparable masses (within the region where stellar kinematics indicators can be measured) and are thus expected to heavily influence each other.

Therefore, we start out with a family of two-component spherical models where each component is described by a distribution function of the f_∞-form:

$$f_L = A_L(-E)^{3/2} \exp\left[-a_L E - c_L J^2/2\right], \quad (1)$$

$$f_D = A_D(-E)^{3/2} \exp\left[-a_D E - c_D J^2/2\right], \quad (2)$$

where $E = v^2/2 + \Phi$ is the specific energy and $J^2 = r^2 v_T^2$ is the specific angular momentum. The distribution functions f_L and f_D are taken to vanish for $E \geq 0$. With this choice, we can imagine varying the "temperature," the amount, and the radial scale of the dark matter by changing the ratios a_D/a_L, A_D/A_L, and c_D/c_L.

An extensive survey is required to study how the physical properties of the models are constrained by self-consistency, which is imposed by the Poisson equation for the gravitational potential Φ shared by the two components.

This is a survey of models with four free parameters. We start with seven dimensional parameters a_L, a_D, c_L, c_D, A_L, A_D, and the value of the central gravitational potential $\Phi(0)$. Two of these can be fixed by choosing the scale length and the total mass of the model. A third parameter can be eliminated by solving the Poisson equation under the appropriate boundary conditions. A convenient choice of dimensionless parameters is a_D/a_L, c_D/c_L, A_D/A_L, $\Psi = -a_L\Phi(0)$, which are taken to be positive. We discuss their physical meaning in the next section.

Taking into account the existence of "conjugate" models, that is, those that are obtained by exchanging the luminous with the dark component, for a complete survey of solutions it is sufficient to take $a_D/a_L < 1$. Models with $a_D/a_L = 1$ and $c_D/c_L = 1$, or models with either A_L or A_D equal to zero are all equivalent to the reference one-component f_∞-models. Here we do not survey models with $\Psi < 0$ or $a_D < 0$ because they are expected to be dynamically unstable. (In fact, models with "negative temperature" [Merritt, Tremaine, & Johnstone 1989] are characterized by a very high degree of radial anisotropy which makes them violently unstable even in the presence of a halo [Stiavelli & Sparke 1991].)

We should stress that the models considered in this paper while allowing for some variations in the distribution of stellar orbits, do *not* have *arbitrary* "pressure" profiles for the two components; in particular, they are all isotropic in the central parts and dominated by radial orbits in the outer regions. This choice of focus, which excludes many other options, such as models dominated by circular orbits, is made on purpose because we would like to study models consistent with the most widely accepted ideas on galaxy formation, that is, dissipationless collapse (van Albada 1982) and merging (see, e.g., Barnes 1989). On the other hand, the detailed *analytical form* of distribution function for the models selected by the physical picture that we adopt is by no means unique (Bertin & Stiavelli 1989). Thus, in order to test the generality of our approach we have also considered in some detail models described by other distribution functions that also incorporate the essential features of collisionless collapse (Stiavelli & Bertin 1987, equation 9). Some of these models will be used in Paper II to test our luminous-dark decomposition on "simulated observations."

In conclusion, we do not claim full completeness of analysis in our investigation of two-component models, but only physical plausibility and sufficient generality of the models that we focus on. This paper will then provide the theoretical basis for

one way of modeling elliptical galaxies and measuring M/L ratios as illustrated in the following Paper II.

3. THE PARAMETER SPACE FOR THE $(f_\infty + f_\infty)$ MODELS AND ITS PHYSICAL MEANING

The dimensionless parameters a_D/a_L, c_D/c_L, A_D/A_L, and Ψ are directly related to the physical properties of the model. We define $\bar{\sigma}_r(r)$, $\bar{\sigma}_T(r)$, and $\bar{\sigma}(r) = \sqrt{(\bar{\sigma}_r^2 + \bar{\sigma}_T^2)/3}$ as the radial, tangential, and unprojected (average over the spatial directions) velocity dispersion, respectively, and $\sigma(R)$ as the velocity dispersion of a given component projected along the line of sight at projected distance R from the center.

For high values of Ψ ($\Psi \gg 1$, $\Psi \gg a_L/a_D$) we obtain the following relations for the central velocity dispersion and density ratios:

$$\frac{\bar{\sigma}_L(0)}{\bar{\sigma}_D(0)} \sim \left(\frac{a_D}{a_L}\right)^{1/2}, \tag{3}$$

$$\frac{\rho_L(0)}{\rho_D(0)} \sim \frac{A_L}{A_D}\left(\frac{a_D}{a_L}\right)^{3/2} \exp\left[\Psi\left(1 - \frac{a_D}{a_L}\right)\right]. \tag{4}$$

Note that for $0.25 \leq a_D/a_L \leq 1$, which is the range considered in the survey of models described in the next section, we have $\bar{\sigma}_D(0) \leq 1.75\bar{\sigma}_L(0)$. In a *hot* dark matter scenario, the dark component should have a velocity dispersion much higher than that of the luminous component. Thus, a very low value of a_D/a_L is needed to produce an $(f_\infty + f_\infty)$-model with this property. In contrast, models with $a_D/a_L \lesssim 1$ have a $\bar{\sigma}_L(0)/\bar{\sigma}_D(0)$ ratio similar to what we can expect in a *cold* or *warm* dark matter scenario.

The value of c_D/c_L fixes the ratio r_{aL}/r_{aD} of the anisotropy radii of the luminous and of the dark components. The anisotropy radius r_a is defined as the location where the anisotropy parameter $\alpha(r) = 2 - \bar{\sigma}_T^2(r)/\bar{\sigma}_r^2(r)$ equals unity (cf. van Albada 1982). In contrast with the estimates given by equations (3)–(4), the relation between c_D/c_L and the ratio r_{aL}/r_{aD} depends on the global properties of the self-consistent solutions. On the basis of the survey of the $(f_\infty + f_\infty)$ models to be described in the next section, we find that a very good power-law fit for the anisotropy ratio r_{aL}/r_{aD} is given by the relation:

$$\frac{r_{aL}}{r_{aD}} \approx 1.1\left(\frac{c_D}{c_L}\right)^{0.8}. \tag{5}$$

Once the Poisson equation has been solved, all the physical properties of the models can be derived; a synthetic description of the global features of these models can be given in terms of a few physical parameters in addition to r_{aL}/r_{aD}, such as:

1. The ratio r_L/r_D of the half-mass radii of the two components.
2. The ratio M_L/M_D of the total masses of the two components.
3. The flatness parameter of the (unprojected) velocity dispersion profile of the luminous component $\bar{\sigma}_L(3r_L)/\bar{\sigma}_L(0)$.
4. The flatness parameters of the circular velocity profile $V(3r_L)/V_{\max}$, where $V(r) = \sqrt{r(d\Phi/dr)}$ measures the gravitational force field of the model with maximum value $V_{\max}$.
5. The "luminosity" parameter:

$$\chi^2_{10} = \sum_{r=r_L/10}^{10r_L} \left[\frac{\rho_L(r) - \rho_J(r)}{\rho_L(r)}\right]^2 \Big/ N, \tag{6}$$

which we introduce in order to measure the departures from the $R^{1/4}$ law of the density of the luminous component. In equation (6) N is the number of points considered, and for simplicity the density consistent with the $R^{1/4}$ profile is approximated by means of the function ρ_J (Jaffe 1983), scaled to have the same half-mass radius and the same density at such radius.

4. A SURVEY OF $(f_\infty + f_\infty)$ MODELS

We have solved the Poisson equation numerically under the natural boundary conditions (see Saglia 1990), using the algorithms described in Appendix A, for 10,000 values of the parameters a_D/a_L, c_D/c_L, A_D/A_L, Ψ. For a given set of dimensional parameters a_D, a_L, A_D, A_L, Ψ/a_L, and c_D, our code computes a value of c_L (if it exists) which produces an equilibrium model satisfying the virial theorem with a given accuracy ($|1 - 2K/|W|| < 10^{-4}$).

The explored region of the parameter space is defined as follows. Twenty different values of c_D and A_D ($30 \leq c_D \leq 600$, $1 \leq A_D \leq 39$) and five different values of a_D and Ψ ($0.5 \leq a_D \leq 1.5$, $8 \leq \Psi \leq 24$), all uniformly spaced, have been considered, setting our units so that $A_L = 1$, $a_L = 2$ and the gravitational constant $G = 1/4\pi$. The adopted grid covers a wide region of the allowed parameter space, with central density ratio $\rho_L(0)/\rho_D(0)$ ranging from 10^{-1} to 10^7. In particular, high values of Ψ have been focused on, since the luminous component of the $(f_\infty + f_\infty)$ models follows the $R^{1/4}$ law only if it is sufficiently centrally concentrated.

4.1. *The Set of Accepted Solutions: "Normal" and "Reverse" Models*

Out of the 10,000 models calculated, only 2939 solutions were accepted. In the remaining cases, the numerical routines either did not converge or led to solutions that were judged to be inaccurate.

We define as *normal*, models with $r_L/r_D < 1$, and as *reverse*, models with $r_L/r_D > 1$. A *normal* model with parameters a_D/a_L, c_D/c_L, A_D/A_L, and Ψ is "conjugate" to the *reverse* model with parameters a_L/a_D, c_L/c_D, A_L/A_D, and $\Psi a_D/a_L$. We found 852 *normal* models and 2087 *reverse* models. *Normal* models are interesting for the description of elliptical galaxies with dark matter, since they possess a highly concentrated luminous component and a more diffuse dark halo. *Reverse* models have in general a dark component with small or insignificant mass. Thus, in their observable properties they are very similar to the one-component f_∞-models with the same value of Ψ.

Some properties of the equilibrium models can be described by the following interpolation formulae:

$$\frac{r_L}{r_D} \approx 1.6\left(\frac{c_D}{c_L}\right)^{0.45}\left(\frac{a_D}{a_L}\right)^{0.8}\left(\frac{A_D}{A_L}\right)^{-0.3}, \tag{7}$$

$$\frac{M_L}{M_D} \approx 1.8\left(\frac{c_D}{c_L}\right)^{0.3}\left(\frac{a_D}{a_L}\right)^{-0.2}\left(\frac{A_D}{A_L}\right)^{-0.8}. \tag{8}$$

These formulae hold essentially for all values of Ψ for the normal models of our survey, although with a larger scatter with respect to relation (5).

The 2939 accepted models described above cover a wide region of the physical parameter space. The $r_L/r_D - M_L/M_D$ plane is covered almost uniformly, except that models with low r_L/r_D ratios have only low M_L/M_D values. It is possible to construct models with a less massive and more diffuse dark component by choosing lower values of the parameter a_D/a_L ($a_D/a_L < 0.25$). In Figure 1 we illustrate the range of properties

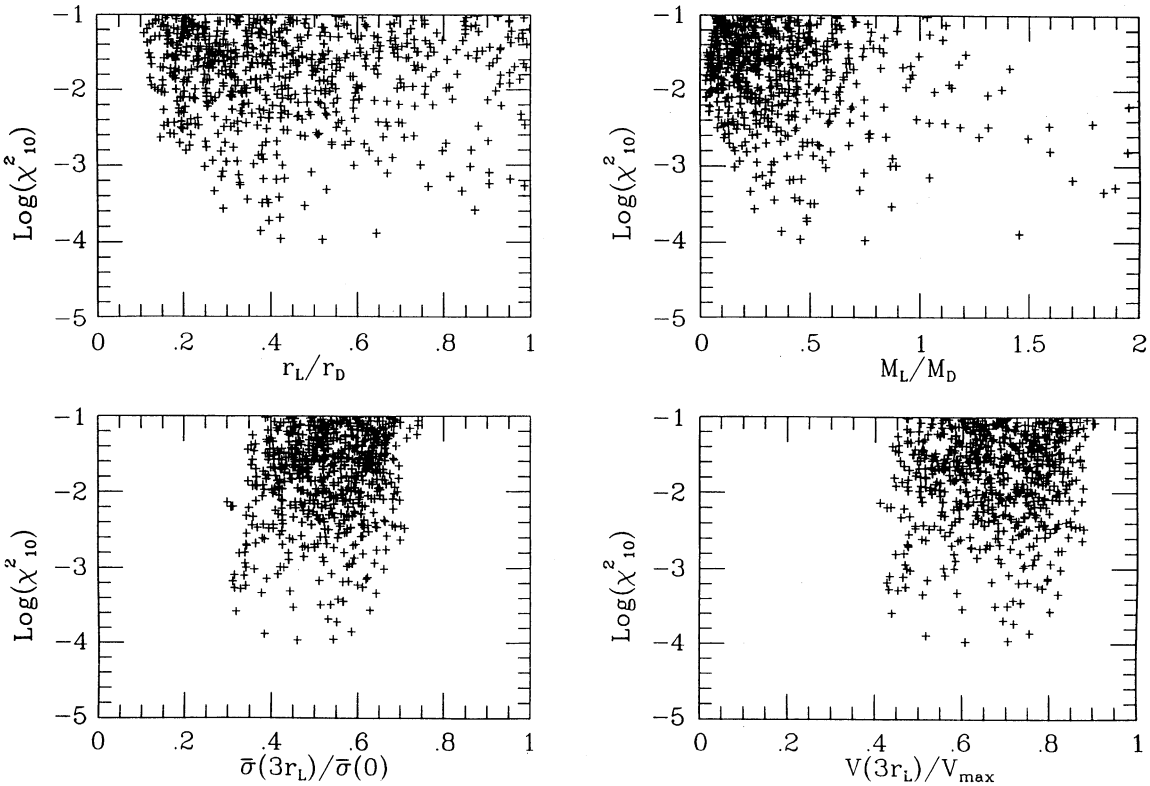

FIG. 1.—"Luminosity parameter" is plotted vs. some key mass and kinematical quantities for the two-component *normal* models

probed by our family of models for other physical parameters as a function of the value of the χ^2_{10} parameter. From these plots it follows that we have constructed a set of models with a luminous component following the $R^{1/4}$ law ($\log \chi^2_{10} < -1$) and with a large spread in the dark mass content and in the mass distribution. From the same plots it follows that a wide class of velocity dispersion profiles has been obtained, from the steeply declining case [$\bar{\sigma}_L(3r_L)/\bar{\sigma}_L(0) = 0.3$], to the nearly flat behavior [$\bar{\sigma}_L(3r_L)/\bar{\sigma}_L(0) = 0.7$]. Finally, these models show quite a variety of circular velocity profiles. In conclusion, our set of two-component models can describe elliptical galaxies with a moderately massive and diffuse dark halo with slowly declining velocity dispersion profiles and nearly flat circular velocity profiles.

4.2. *Three Representative Classes of Two-Component Models*

The models that we have constructed can be roughly grouped in three classes on the basis of the relative importance and distribution of their luminous and dark components. These classes are well illustrated by three representative models ($N = 402$, 1857, and 9382; see Fig. 2).

The *reverse* model $N = 402$ ($\Psi = 12$, $a_D = 0.5$, $A_D = 1$, $c_D = 150$, $c_L = 10$) has a small amount of dark matter ($M_L/M_D = 8.5$) and thus is very similar to the one-component $\Psi = 12$ model. The densities of the luminous and dark components decrease as r^{-4} in the outer regions ($r > r_L$, $r_L = 0.41$, $r_L/r_D = 1.4$), while for $10^{-3} r_L < r < r_L$ we have $\rho_L \sim r^{-2}$, $\rho_D \sim r^{-1.1}$. In the very central regions ($r < 10^{-3} r_L$) there is a flat core. The model has a Keplerian circular velocity profile. Models with a low content of dark matter (in particular, most of the *reverse* models) show similar properties.

The model $N = 1857$ ($\Psi = 12$, $a_D = 0.5$, $A_D = 23$, $c_D = 560$, $c_L = 353.7$) has a larger fraction of dark matter ($M_L/M_D = 0.27$), but the dark halo becomes dominant only in the outer regions ($r > r_L$, $r_L = 0.026$, $r_L/r_D = 0.29$). For $0.04\ r_L < r < r_L$ we find $\rho_L \sim r^{-2}$, $\rho_D \sim r^{-1.1}$, while for $r > r_L$, $\rho_L \sim r^{-4}$ and finally for $r > r_D$, $\rho_D \sim r^{-4}$ also. The circular velocity profile has a central peak due to concentration of the luminous component; it stays flat in the region $0.3r_L < r < 1.6r_L$ and begins to decrease at greater radii. Notice how the flat part of the circular velocity profile is produced by the combination of the declining contribution of the luminous component and the rising curve caused by the dark halo.

The model $N = 9382$ ($\Psi = 12$, $a_D = 1.5$, $A_D = 33$, $c_D = 420$, $c_L = 1336$, $r_L = 0.022$, $r_L/r_D = 0.29$) is dominated by dark matter ($M_L/M_D = 0.03$). In the region $5 \times 10^{-3} r_D < r < r_D$ we find $\rho_L \sim r^{-2.7}$, $\rho_D \sim r^{-2}$, while in the outer regions $\rho_L \sim r^{-4}$, $\rho_D \sim r^{-4}$. Outside the inner peak, the circular velocity profile is monotonically decreasing.

Since the transition among these classes of models is smooth, we can identify systems with intermediate features. Models, some of which reverse, with a conspicuous amount of dark matter inside R_e belong to these intermediate categories.

4.3. *Projections along the Line of Sight*

In order to compare theoretical models with observations (as will be done in Paper II), it is necessary to project the relevant physical properties of the models. We have computed the surface density (normalized to the densities at $R = R_e$) and the velocity dispersion profile projected along the line of sight for the luminous and dark component of all the models that we have determined.

For each *normal* model we have computed the parameter χ^2_P

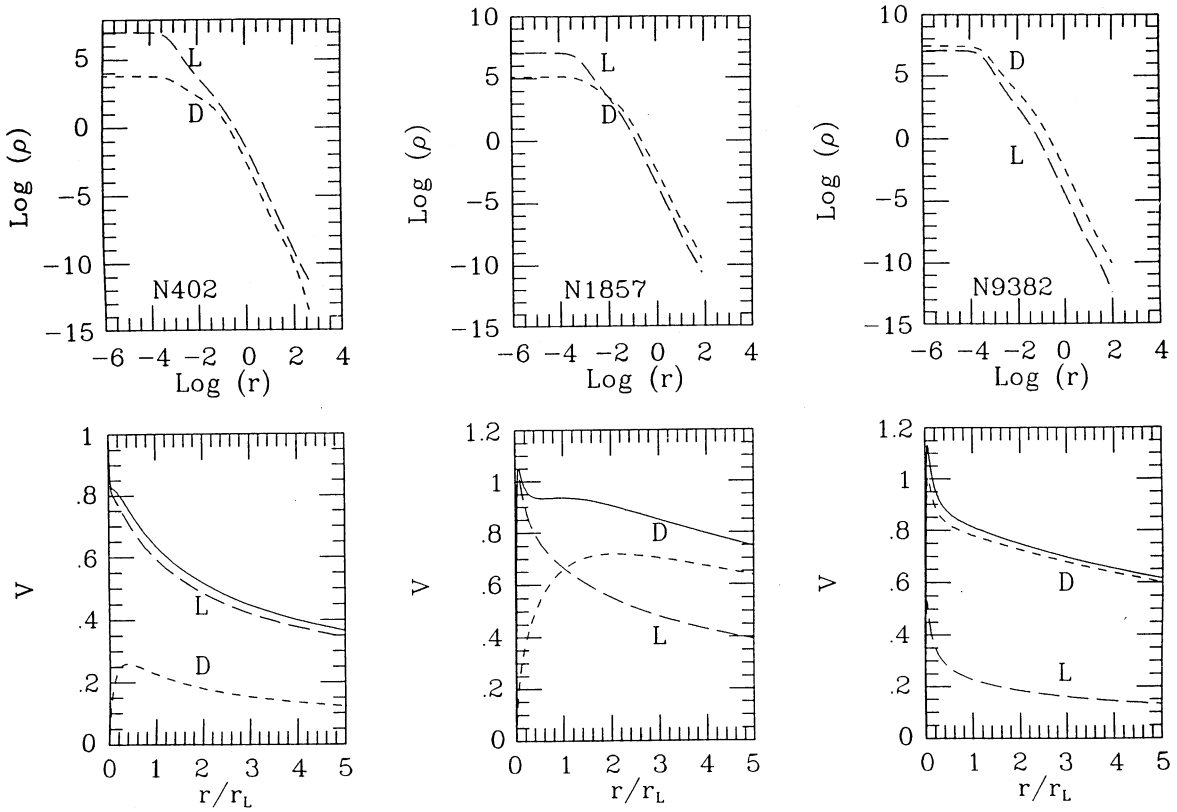

FIG. 2.—Upper row: volume densities of the luminous and of the dark components for three representative models (see discussion in § 4.2). Bottom row: circular velocity profile for the same models separated into the contribution of the luminous and of the dark components. Here the radial distance is normalized to the half-mass radius of the luminous component. All velocities are given in model units.

as a direct measure of the departures from the $R^{1/4}$ law:

$$\chi_P^2 = \sum_{R=R_e/10}^{3R_e} [\mu_L(R) - \mu_{1/4}(R)]^2/N \,, \qquad (9)$$

where $\mu_L = -2.5 \log \Sigma(R)$ is the surface density of the luminous component of the model expressed in magnitudes, $\mu_{1/4}(R)$ is the corresponding magnitude of the $R^{1/4}$ law and N is the number of points considered in the sum. A reasonable correlation is found between χ_P^2 and χ_{10}^2.

In Figure 3 we show the position of the *normal*, minimum-halo (see following § 5) models with $\chi_{10}^2 < 0.01$ on the planes $M_L/M_D - M_L/[R_e\sigma_L^2(0)/G]$ and $M_L/M_D - (M_L$

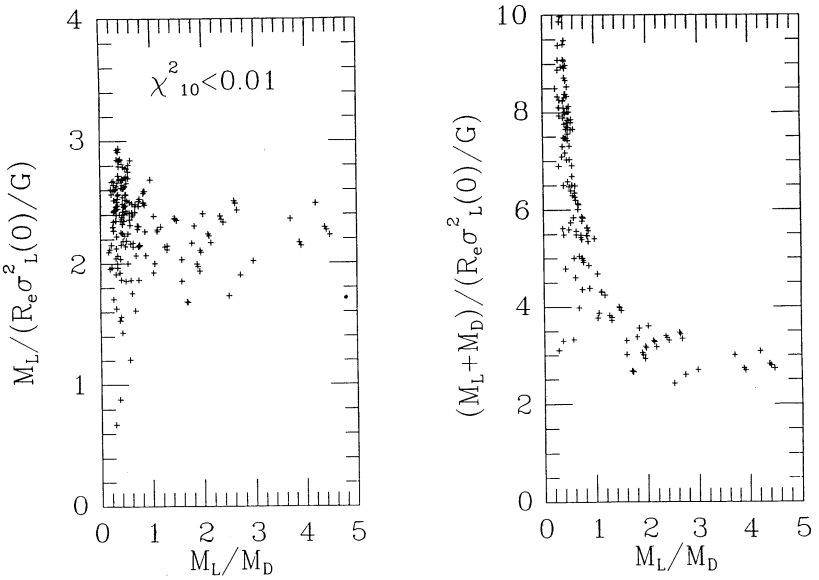

FIG. 3.—Correlations between M_L/M_D and the quantities $M_L/[R_e\sigma_L^2(0)/G]$ (*left frame*) and $(M_L + M_D)/[R_e\sigma_L^2(0)/G]$ (*right frame*) for normal, minimum-halo models with $\chi_{10}^2 < 0.01$. The quantity $R_e\sigma_L^2(0)/G$ clearly underestimates the total mass of the model if $M_L/M_D < 1.5$.

$+ M_D)/[R_e \sigma_L^2(0)/G]$. These plots show that the quantity $2R_e\sigma_L^2(0)/G$, often used to estimate the mass of elliptical galaxies, can give the luminous mass of the objects with $\approx 50\%$ accuracy, but strongly underestimates their total mass, if a massive ($M_L/M_D < 1.5$) dark component is present.

5. MINIMUM-HALO MODELS

There are two obvious limiting cases where significant amounts of dark matter are expected to coexist with the stellar component without distorting the observed luminosity profile. The first possibility is that the dark component is distributed exactly as the luminous component. In this case, only the high value of the derived (constant) M/L ratio may suggest that dark matter is present.

The second and more interesting possibility is to assume that dark matter is diffuse (i.e., $r_D > r_L$), with a central density much smaller than that of the luminous component. In this case, the "dark" contribution to the potential becomes important only in the external regions of the galaxy, and the density distribution of the dark halo is different from that of the stellar component of the galaxy (see, e.g., the model $N = 1857$ described in § 4.2). Here the M/L ratio is an increasing function of radius.

To be more specific, given a two-component model $\bar{f} = \bar{f}_L + \bar{f}_D$ in the self-consistent potential, it is always possible to construct models with the same observables (projected luminosity profile, projected velocity dispersion profile, and circular velocity) but with different amounts of dark matter. For this purpose, it is sufficient to decrease the (M/L) ratio of the stellar component by "moving" part of the mass from the luminous to the dark component:

$$\bar{f} = \bar{f}'_L + \bar{f}'_D = \lambda\bar{f}_L + [\bar{f}_D + (1-\lambda)\bar{f}_L], \quad \text{with } 0 \le \lambda \le 1. \tag{10}$$

This shows that if we find a model $\bar{f} = \bar{f}_L + \bar{f}_D$ that gives a reasonable fit to the data, we can always refer to a model that equally fits the data but has a larger amount of "dark" matter. A few of these models may happen to be well approximated by models of our class, that is, they may have $\bar{f}'_D$ approximated by an f_∞ function.

We note that moving in the opposite direction, that is, that of *increasing* the amount of luminous matter while keeping the same observable profiles is not always possible. If one considers the symmetric procedure defined by exchanging L and D in equation (10), the observable profiles are likely to be changed because we now have $\bar{f}'_L = \bar{f}_L + (1-\lambda)\bar{f}_D$. On the other hand, if one considers $\lambda \ge 1$ in equation (10), for sufficiently large values of λ the function $\bar{f}'_D$ becomes *negative* and therefore unphysical. On this basis we may define the minimum halo solution for a given object fitted by a model with $\bar{f} = \bar{f}_L + \bar{f}_D$, as that obtained from equation (10) with the largest $\lambda \ge 1$ and $\bar{f}'_D$ positive everywhere. For our $(f_\infty + f_\infty)$-models with $a_L \ge a_D$ and $c_L \ge c_D$ we have

$$\lambda_{\max} = 1 + \frac{A_D}{A_L} \exp\left[-\left(1 - \frac{a_D}{a_L}\right)\Psi\right]. \tag{11}$$

For the models with $c_L < c_D$, $\lambda_{\max} = 1$. The numerical survey has explored models with $\lambda_{\max} \le 6$. Models with high Ψ, low a_D/a_L, or low A_D/A_L values have $\lambda \approx 1$ and consequently have a minimum halo.

Such a minimum halo solution may or may not belong to the class of models investigated in our survey. In any case one should check that the new function $\bar{f}'_D$ does not show peculiar features that would not be reasonably associated with one "homogeneous" component.

5.1. *Limits on the Amount of Dark Matter Inside R_e*

For a class of models for which the luminous component follows the $R^{1/4}$ law and the dark component has a diffuse distribution, we can derive a useful relation between the velocity dispersion profile and the amount of dark matter as a function of radius. In fact, the Jeans equation for the luminous component, under the assumption that the dark component is insignificant at small radii, requires that the central velocity dispersion $\bar{\sigma}_L(0)$ be related to the total mass M_L and to the half-mass radius r_L according to the relation

$$\bar{\sigma}_L^2(0) = \frac{GM_L}{2r_L}. \tag{12}$$

For an $R^{1/4}$ law density profile the density gradient and the cumulative mass profile $M_L(r)$ are also determined. Then the Jeans equation requires

$$GM(r) = 3r\bar{\sigma}_{rL}^2\left[\frac{2(r_L + 2r)}{3(r_L + r)} - \frac{\alpha}{3} - \frac{1}{3}\frac{d\ln\bar{\sigma}_{rL}^2}{d\ln r}\right], \tag{13}$$

where $M(r) = M_L(r) + M_D(r)$ and $\bar{\sigma}_{rL}^2 = \langle v_r^2\rangle_L$. For an $R^{1/4}$ profile we have $r_L \sim 1.32R_e$ (where R_e is the radius enclosing half of the projected mass), so that $M_L(R_e) \approx 0.43M_L$. Thus:

$$\frac{M_D(R_e)}{M_L(R_e)} \approx 2.5\,\frac{\bar{\sigma}_{rL}^2(R_e)}{\bar{\sigma}_{rL}^2(0)}\left(1 - 0.35\alpha - 0.35\,\frac{d\ln\bar{\sigma}_{rL}^2}{d\ln r}\right) - 1. \tag{14}$$

For many of the models of our survey for $r \lesssim R_e$ we have $\alpha \approx 0$, $d\ln\bar{\sigma}_{rL}^2/d\ln r \approx -0.5$, and the value of $\bar{\sigma}_{rL}^2(R_e)/\bar{\sigma}_{rL}^2(0)$ exceeds by 15% the value of $\sigma_L^2(R_e)/\sigma_L^2(0)$ for the projected quantities. On this basis we can argue the following estimate:

$$\frac{M_D(R_e)}{M_L(R_e)} \approx 3.5\,\frac{\sigma_L^2(R_e)}{\sigma_L^2(0)} - 1, \tag{15}$$

which now relates the amount of dark matter present inside R_e to the directly observable velocity dispersion profile. Here $\sigma_L(0)$ denotes the velocity dispersion in the vicinity of the center excluding any peculiarities that may be associated with the nucleus. Equation (15) has been derived without assuming any specific form for the distribution functions of the luminous and of the dark components. The only requirements are that the stellar velocity distribution is essentially isotropic in the inner part of the galaxy and that the luminous density follows the $R^{1/4}$ law. Under these hypotheses, a flat velocity dispersion profile traces the presence of a massive dark halo. Note that this estimate of M_D is conservative with respect to the presence of finite rotation of the system, in the sense that, for given observed values of $\sigma_L(R_e)$ and $\sigma_L(0)$, if the object is slightly rotating in the way often observed in ellipticals, then the relation underestimates the $(M_D/M_L)_{R_e}$ ratio.

In Figure 4 we show the properties of the *normal* models of our survey with a projected luminous density that follows with good accuracy the $R^{1/4}$ law ($\chi_{10}^2 < 0.01$) in the plane $\sigma_L^2(R_e)/\sigma_L^2(0)$–$(M_D/M_L)_{R_e}$ Models falling on the relation generally have a diffuse dark component ($r_D > r_L$) with a central density $\rho_D(0)$ much smaller than that of the luminous component. Models with $(M_D/M_L)_{R_e}$ much larger than predicted by equation (15) have instead $\rho_L(0) \approx 1 - 8\rho_D(0)$ and $r_D < 5r_L$. In the central parts of these models the luminous and

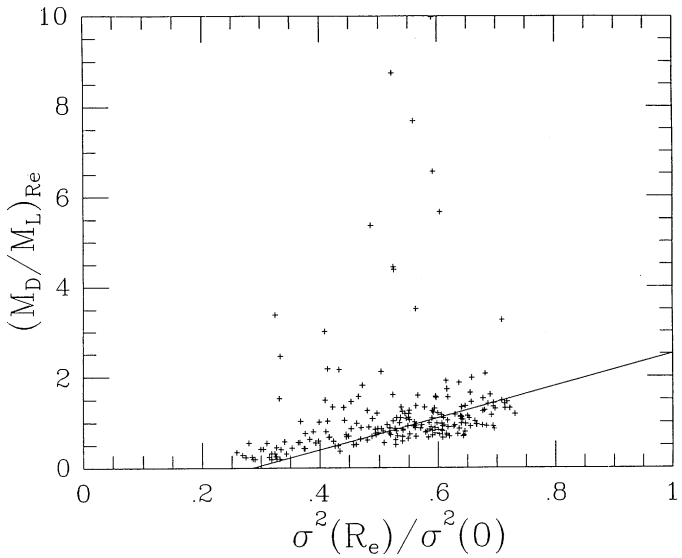

FIG. 4.—Crosses show the normal two-component models with a projected luminosity that follows the $R^{1/4}$ law with a prescribed accuracy ($\chi^2_{10} < 0.01$). The line showing the prediction of eq. (15) is close to the boundary of minimum halo models.

dark density profiles are very close to each other. They have $\lambda_{max} > 1$ and, consequently, following the definition given in § 5, they are not "minimum halo" models.

5.2. *The* $(r_L/r_D, M_L/M_D)$ *Plane*

In order to better characterize the properties of the models of our survey for which the luminous component follows the $R^{1/4}$ law we can refer to the virial relation:

$$2K_L + W_L + W_{LD} = 0\,, \tag{16}$$

where K_L represents the total kinetic energy of the luminous component and

$$W_L = -4\pi G \int_0^\infty r\rho_L(r)M_L(r)dr = -q_L \frac{GM_L^2}{r_L}\,, \tag{17}$$

$$W_{LD} = -4\pi G \int_0^\infty r\rho_L(r)M_D(r)dr = -\frac{GM_L M_D}{r_L}\hat{W}_{LD}\,, \tag{18}$$

represent the gravitational energy terms. The no dark matter case is characterized by $W_{LD} = 0$, $q_L = \frac{1}{2}$. Since the dark component corresponds to a low-Ψ model (if $a_D < a_L$), we may argue that its mass distribution is reasonably represented by a density of the form $\rho_D \propto (r_0^2 + r^2)^{-2}$, with $r_0 \approx 0.45 r_D$. Then we can estimate the interaction term W_{LD} with the following interpolation for the interaction integral:

$$\hat{W}_{LD} \approx \frac{1}{2\pi}\frac{r_L}{r_D}\left[1 + 1.37\left(\frac{r_L}{r_D}\right)\right]. \tag{19}$$

For the class of models that preserve the $R^{1/4}$ law, W_L is practically unchanged with $q_L \approx \frac{1}{2}$, while the presence of the interaction term W_{LD} is balanced by an increase in the kinetic

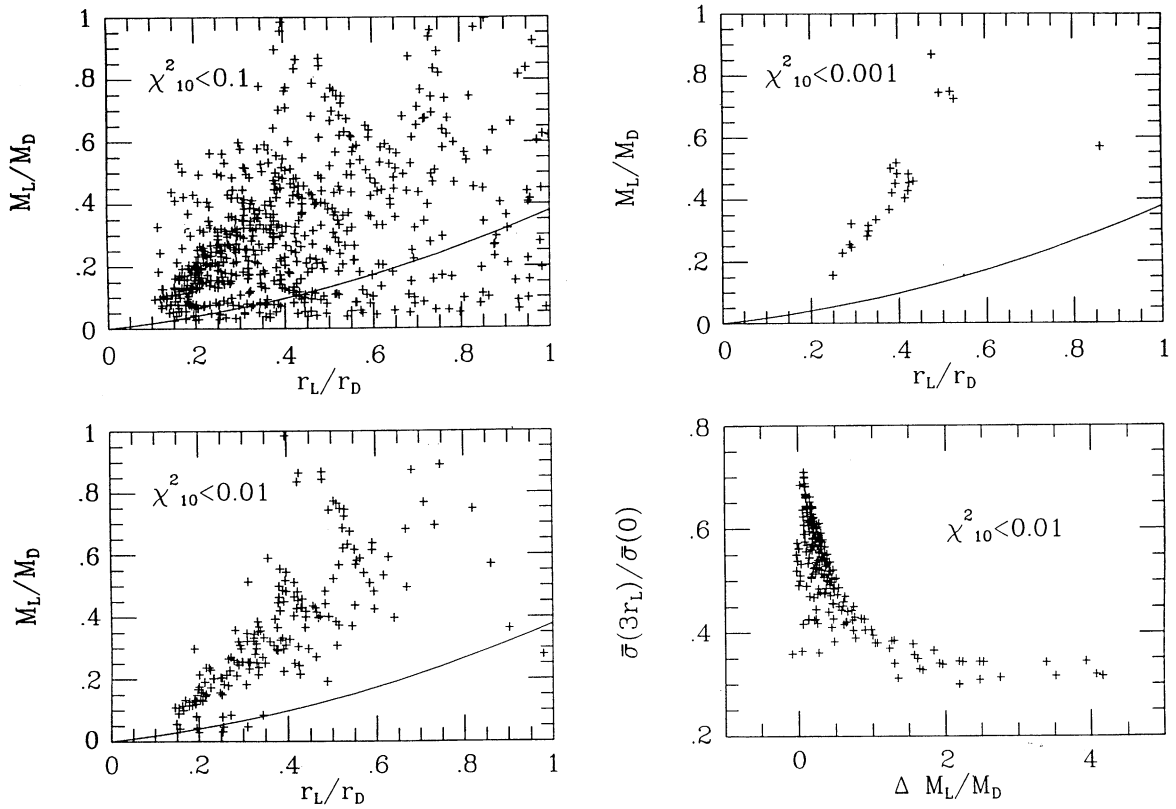

FIG. 5.—Position in the $(r_L/r_D, M_L/M_D)$ plane of the two-component models with a projected luminosity that follows the $R^{1/4}$ law with prescribed accuracy ($\chi^2_{10} < 0.1, 0.01, 0.001$: *upper left*, *bottom left*, and *upper right*, respectively). The line shows the constraint given by eq. (21) argued on the basis of the virial theorem. In the bottom right frame we show the correlation between the difference $\Delta M_L/M_D = M_L/M_D - (M_L/M_D)_{vir}$, where $(M_L/M_D)_{vir}$ is given by the right-hand side of eq. (21), and the flatness parameter of the velocity dispersion profile, for normal models with $\chi^2_{10} < 0.01$. Note that models with low $\Delta M_L/M_D$ values have flatter velocity dispersion profiles.

energy content K_L (see also relation [15]). If we set as an upper limit for K_L the value $(3/2)M_L\bar{\sigma}^2_{rL}(0)$ that would hold for a flat dispersion profile, we obtain the following inequality

$$2K_L = \frac{1}{2}\frac{GM_L^2}{r_L} + \frac{GM_L M_D}{r_L}\hat{W}_{LD} < \frac{3}{2}\frac{GM_L^2}{r_L}, \qquad (20)$$

that is,

$$\frac{M_L}{M_D} > \frac{1}{2\pi}\frac{r_L}{r_D}\left[1 + 1.37\left(\frac{r_L}{r_D}\right)\right]. \qquad (21)$$

Therefore in the $(r_L/r_D, M_L/M_D)$ plane, models following the $R^{1/4}$ law are expected to fall above a parabola, and those models that are close to it are expected to have the flattest velocity dispersion profile (see Fig. 5). The empty region in the upper left part of the plane can be interpreted partly by the limited region of parameter space explored and partly by the fact that those models would have a large interaction term of the luminous on the dark component ($|W_{DL}| \gtrsim |W_D|$). It appears that taking $|W_{DL}| < |W_D|$ goes in the direction of identifying a narrow strip of models that are best fitted by the $R^{1/4}$ law (i.e., $\chi^2_{10} < 0.001$; see Fig. 5, *upper right frame*).

6. CONCLUSIONS

A detailed analysis of the properties of a family of self-consistent, spherical, two-component models of elliptical galaxies has shown that a large set of models exists characterized by the presence of a sizeable amount of dark matter, photometric profiles well-fitted by the $R^{1/4}$ law, and circular velocity and velocity dispersion profiles both fairly flat and featureless.

The distribution function on which the models are based had been shown previously to produce one-component models with the $R^{1/4}$ law as a built-in property (Stiavelli & Bertin 1985). This property is found to be preserved even when the presence of a massive halo is included self-consistently. Both the photometric and the kinematic "conspiracies," neither of which has been imposed a priori, seem to be a natural consequence especially when dark matter has a distribution more diffuse than that of the stellar component.

The present study is mostly based on dynamical arguments on the properties of equilibrium configurations. It remains to be investigated how such equilibria can be obtained as the end product of galaxy formation processes. This line of research is being pursued with the device of N-body simulations.

The models are characterized by a wide range in the ratios of scale lengths and masses, so that their application to the modeling of elliptical galaxies seems to be justified. The major application is to galaxies with dark matter. By fitting the models to observed photometric and kinematical profiles of individual galaxies it is possible to set constraints on the presence and extent of dark halos in these objects. Paper II is devoted to such application.

However, other applications of this approach are possible. The two components may in fact be taken to represent the stellar component and the system of globular clusters in a giant elliptical galaxy, or, alternatively, two different stellar populations in a galaxy with color and metallicity gradients, or, possibly, two distinct stellar populations to represent the observed properties of cD galaxies. Of course for these new cases, the choice of the relevant distribution functions should be carefully examined.

This work has been partially supported by MURST and CNR of Italy. R. P. S. gratefully acknowledges ESO for the hospitality extended to him while part of this work was carried out.

APPENDIX A

NUMERICAL METHODS

The 2939 accepted two-component models described in the paper have been calculated on the VAX 8650 of the Scuola Normale Superiore with a program extensively described by Saglia (1990), with each model identified by a progressive number $N = 2000(i_{a_D} - 1) + 100(i_{c_D} - 1) + 5(i_{A_D} - 1) + i_\Psi$, where $i_{a_D} = 1, 2, \ldots 5$, $i_{c_D} = 1, 2, \ldots 20$, $i_{A_D} = 1, 2, \ldots 20$, $i_\Psi = 1, 2, \ldots 5$, and $a_D(i_{a_D}) = 0.5 + 0.25(i_{a_D} - 1)$, $c_D(i_{c_D}) = 30i_{c_D}$, $A_D(i_{A_D}) = 1 + 2(i_{A_D} - 1)$, $\Psi = 8 + 4(i_\Psi - 1)$.

The Poisson equation is solved by using an iterative shooting method with superlinear convergence. The adopted integration scheme is a fourth-order Adams-Bashfort method (see Press et al. 1985) with a fourth-order Runge-Kutta scheme providing the necessary initialization values. The moments of the distribution functions are computed by using an eight-point Gaussian integrator.

The numerical accuracy of the code has been tested in several ways. Essentially identical results are found by solving the differential equation with the Runge-Kutta method all the way through. Minor changes are observed when the integrations are performed with 12- or 24-point Gaussian integrators. However, the eight-point integrator is probably inadequate for the calculation of very low-density, low-a_D models. In addition, the radial grid used in the calculation has been found to be not sufficiently fine for some of the models with higher central densities and higher Ψ values (i.e., $\Psi = 24$).

The algorithm, when applied to the one-component f_∞ sequence, is able to find correctly the unique value of c associated with a model of given Ψ. The initial guess for c can be varied considerably without affecting the final answer. When applied to the problem of two-component models, the algorithm cannot recognize the possible presence of multiple solutions for c_L. By considering a set of parameters for which two solutions for c_L were known to exist ($a_L = 1.5$, $a_D = 2$, $c_D = 0.1966$, $A_L = 9$, $A_D = 1$, $\Psi = 9$), we have tested that the algorithm can determine one of the two solutions ($c_L = 240$) only when the starting value c_L^s is close to 240 ($239 \leq c_L^s \leq 244$). For other values of c_L^s the algorithm always finds the second solution $c_L = 200$.

For some models with $a_D/a_L = 0.5$–0.68 the code finds solutions with very high values of c_L ($c_L = 10^8$–10^9). Since the f_∞ distribution functions of equations (1) and (2) are set to zero for numerical reasons when the arguments of the exponential functions are lower than -60, these models are certainly inaccurate and have not been considered further in the analysis.

Truncated solutions, with finite radial extent, are easily computed. They have not been considered in the paper since their properties closely resemble those of the models of infinite extent whenever their truncation radius is large. On the other hand, they are not well fitted by the $R^{1/4}$ law when their truncation radius is small.

APPENDIX B

SOME LIMITATIONS OF THE PRESENT SURVEY

A few questions that need to be addressed are related to the effect of adding new ingredients to the physical picture outlined in § 2. An extensive study of these issues is beyond the scope of this paper. Here we report on the properties of some models outside the main survey and on the effect of rotation.

B1. A FEW MODELS OUTSIDE THE MAIN SURVEY

In order to complete our survey, we have also computed a few models with low values of a_D and a few others with $a_D = a_L$. Models with high-velocity dispersion for the dark component (i.e., small a_D) are hard to explore extensively, since they require the use of higher order Gaussian integrators, and consequently large amounts of CPU time. These models tend to have massive and diffuse dark halos and are characterized by very flat circular velocity and velocity dispersion profiles.

Other models outside the main survey have $a_D = a_L$. The interest in these lies in the fact that they represent the case where the dark matter is coldest. The density distribution of the two components is similar for $r < r_L$, so that the mass-to-light ratio is approximately constant at small radii. All the computed models have a massive dark component ($M_L/M_D < 1$). The values of the ratios r_L/r_D and M_L/M_D correlate (see eqs. [7] and [8]), so that massive halos are also diffuse. Only models with $r_L \approx r_D$ or $r_L < 0.1 r_D$ have $\chi^2_{10} < 0.01$, that is, a good $R^{1/4}$ luminosity profile. In their general properties, these models are found to resemble those with $a_D/a_L = 0.75$.

B2. INFLUENCE OF ROTATION

It is possible to construct (spherical) rotating analogues (Petrou 1983) of the models described so far, by using the distribution function discussed in Stiavelli & Bertin (1985, eq. 5.1), and characterized by two additional parameters: B and Ω. Parameter B

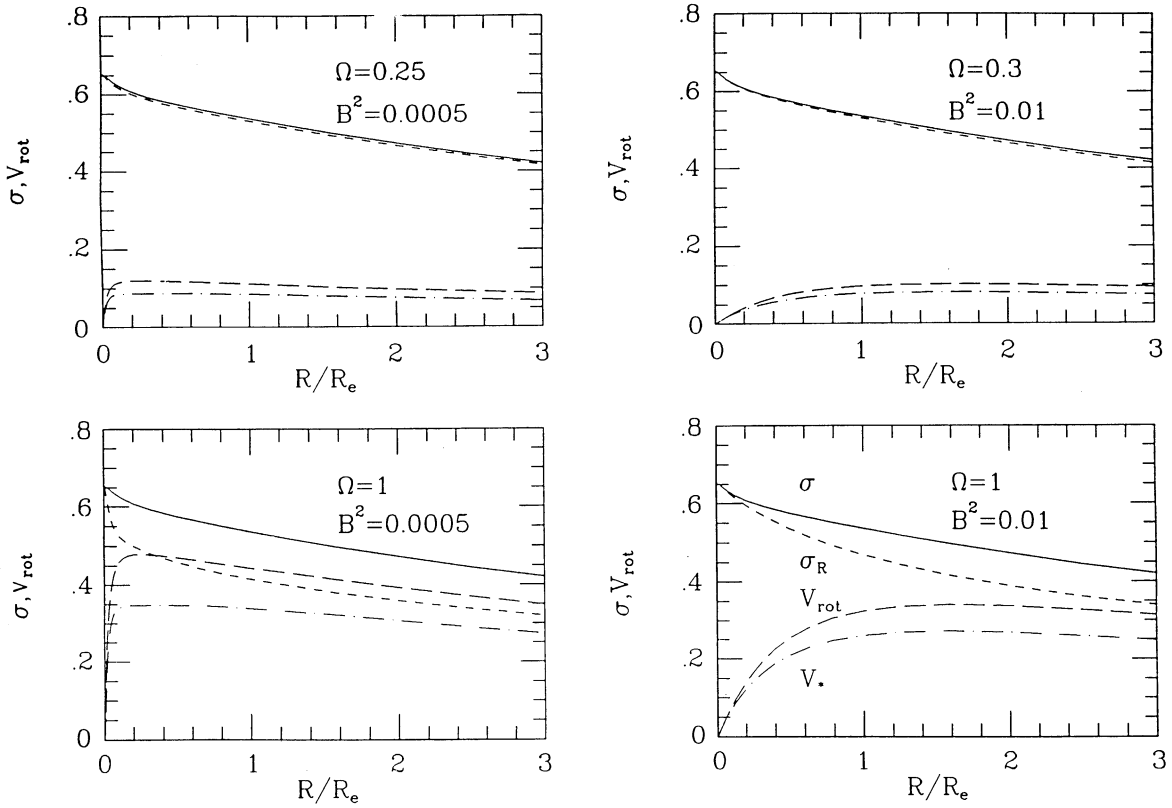

FIG. 6.—Projected rotation curves (*dotted long-dashed lines*) and velocity dispersion profiles (*short-dashed lines*) are plotted for the model $N = 1857R$ modified to include rotation and four values of the parameters defining the rotation curve. The velocity dispersion profile of the nonrotating model (*solid line*) and the unprojected rotation curve (*long-dashed line*) are also shown for comparison. Here the radial distance is normalized to the projected half-mass radius of the luminous component. All velocities are given in model units. Note that the profiles are significantly affected by rotation and projection; in particular, sizeable differences can occur between σ_R and σ, and between V_* and V_{rot}.

defines the shape of the (stellar) rotation curve, and $\Omega(\leq 1)$ the amount of rotation. For the model $N = 1857R$ modified to include rotation, we have computed a few rotation curves for $\Omega = 0.25$, 0.3, 1.0 and for $B^2 = 5 \times 10^{-4}$ and 0.01. These rotation curves are shown in Figure 6 with their projections along a line of sight perpendicular to the rotation axis and with the associated projected velocity dispersions. As is readily seen, models with fast rising rotation curves are characterized by a velocity dispersion profile more peaked toward the center. For Ω close to unity the effect can be quite strong, even when the observed $V_{*\max}/\sigma_L(0)$ is smaller than 0.5.

The influence of rotation on the observed kinematics depends on the specific form of the adopted distribution function. The term $\sigma_L^2(R_e)$ in equation (15) should be replaced by $\sigma_L^2(R_e) + \xi V_*^2(R_e)$, with $\xi \leq 1$. In general, the *measured* mean velocity of the stars V_* would be smaller than the intrinsic unprojected rotation velocity $V_{\rm rot}$, because of the inclination of the axis of rotation with respect to the line of sight, and also as a result of the integration along the line of sight. In addition, the latter effect produces an asymmetric distortion and widening of the line profiles, thus affecting the determination of the velocity dispersion profile (Saglia 1990; Bender 1990).

It is worthwhile to stress that stellar rotation curves, $V_*(R)$, can have a variety of shapes not directly related to the underlying gravitational potential, in contrast to the rotation curve for test particles, such as the H I rotation curve, which is given by the circular velocity $V(R)$ and thus is directly related to the force field.

B3. STABILITY

N-body simulations have been performed to check that the equilibrium models used in this analysis were stable.

REFERENCES

Barnes, J. E. 1989, Nature, 338, 123
Bender, R. 1990, A&A, 229, 441
Bertin, G., Saglia, R. P., & Stiavelli, M. 1988, ApJ, 330, 78
———. 1989, in Astronomy, Cosmology, and Fundamental Physics, ed. M. Caffo et al. (Dordrecht: Kluwer), 303
Bertin, G., & Stiavelli, M. 1984, A&A, 137, 26
———. 1989, ApJ, 338, 723
Binney, J. J., Davies, R. L., & Illingworth, G. D. 1990, ApJ, 361, 78
Canizares, C. R., Fabbiano, G., & Trinchieri, G. 1987, ApJ, 312, 503
de Vaucouleurs, G. 1948, Ann. d'Astrophys. 11, 247
———. 1953, MNRAS, 113, 134
Efstathiou, G., Ellis, R. S., & Carter, D. 1982, MNRAS 201, 975
Fabricant, D., Lecar, M., & Gorenstein, P. 1980, ApJ, 241, 552
Forman, W., Schwarz, J., Jones, C., Liller, W., & Fabian, A. C. 1979, ApJ, 234, L27
Franx, M., & Illingworth, G. 1990, ApJ, 359, L41
Jaffe, W. 1983, MNRAS, 202, 995
Lees, J. F., van Gorkom, J. H., & Knapp, G. R. 1990, BAAS, 21, 1178
Merritt, D., Tremaine, S., & Johnstone, D. 1989, MNRAS, 236, 829
Peletier, R. F., Davies, R. L., Illingworth, G. D., Davis, L. E., & Cawson, M. 1990, AJ, 100, 1091
Petrou, M. 1983, MNRAS, 202, 1209
Press, W. H., Flannery, B. P., Teukolsky, S. A., & Vetterling, N. T. 1985, Numerical Recipes (Cambridge: Cambridge Univ. Press)
Raimond, E., Faber, S. M., Gallagher III, S. J., & Knapp, G. R. 1981, ApJ, 246, 708
Saglia, R. P. 1990, Ph.D. thesis, Scuola Normale Superiore, Pisa
Saglia, R. P., Bertin, G., & Stiavelli, M. 1992, ApJ, 384, 433 (Paper II)
Sancisi, R., & van Albada, T. S. 1987, in Observational Cosmology, ed. A. Hewitt et al. (Dordrecht: Reidel), 699
Sarazin, C. L. 1987, in Structure and Dynamics of Elliptical Galaxies, ed. P. T. de Zeeuw (Dordrecht: Reidel), 179
Schweizer, F., van Gorkom, J. H., & Seitzer, P. 1989, ApJ, 338, 770
Stiavelli, M., & Bertin, G. 1985, MNRAS, 217, 735
———. 1987, MNRAS, 229, 61
Stiavelli, M., & Sparke, L. 1991, ApJ, 382, 466
van Albada, T. S. 1982, MNRAS, 201, 939
van Albada, T. S., Bahcall, J., Begeman, K., & Sancisi, R. 1985, ApJ, 295, 305
van Albada, T. S., & Sancisi, R. 1986, Phil. Trans. R. Soc., Lond., A, 320, 447
van der Marel, R., Binney, J., & Davies, R. L. 1990, MNRAS, 245, 582
van Gorkom, J. H., Knapp, G. R., Raimond, E., Faber, S. M., & Gallagher, J. S. 1986, AJ, 91, 791